Model of a laser heated plasma interacting with walls arising in laser keyhole welding

C. Tix and G. Simon

Institut für Theoretische Physik, Technische Universität Braunschweig, Mendelssohnstraße 3, D-38106 Braunschweig, Germany

In laser welding with laser intensities of approximately 10^{11} W/m^2, a hole, called a keyhole, is formed in the material. In this keyhole a plasma is detected, which is characterized by high pressure as well as being influenced by the boundary of the keyhole. Experimental data on plasma parameters are rare and difficult to obtain [W. Sokolowski, G. Herziger, and E. Beyer, in *High Power Lasers and Laser Machining Technology*, edited by A. Quenzer, SPIE Proc. Vol. 1132 (SPIE, Bellingham, WA, 1989), pp. 288–295]. In a previous paper [C. Tix and G. Simon, J. Phys. D **26**, 2066 (1993)] we considered just a simple plasma model without excited states and with constant ion–neutral-atom temperature. Therefore we neglected radiative transport of excitations and underestimated the ion–neutral-atom temperature and the ionization rate. Here we extend our previous model for a continuous CO_2 laser and iron and take into account radiative transfer of excitations and a variable ion–neutral-atom temperature. We consider singly charged ions, electrons, and three excitation states of neutral atoms. The plasma is divided in plasma bulk, presheath, and sheath. The transport equations are solved with boundary conditions mainly determined through the appearance of walls. Some effort is made to clarify the energy transport mechanism from the laser beam into the material. Dependent on the incident laser power, the mean electron temperature and density are obtained to be 1.0–1.3 eV and 2.5×10^{23}–3×10^{23} m^{-3}. Radiative transport of excitations does not contribute significantly to the energy transport.

PACS number(s): 52.50.Jm, 42.62.Cf, 52.40.Hf

I. INTRODUCTION

When a continuous laser beam with intensity of about 10^{10}–10^{11} W m^{-2} and beam radius of about 10^{-4} m is directed on a metal surface, a hole is formed in the material. In this hole (sometimes called a keyhole) a plasma is detected with electron densities and temperatures of about 10^{23}–10^{24} m^{-3} and 1 eV, respectively [1].

Such a situation arises in laser welding, when a laser is wielded over the contact line of two work pieces. It is observed that the keyhole enhances the energy transfer from the laser beam to the material [2]. The keyhole arises for laser intensities of about 10^9 W m^{-2} and the plasma is observed for intensities of about 10^{10} W m^{-2} [3]. At this threshold intensity the depth of penetration of the laser beam into the material undergoes a large increase which is usually connected with the appearance of the plasma. Typical diameters of the laser beam are in the range of some 10^{-4} m and the keyhole is observed to attain a radius in the same order of magnitude. To get a penetration depth 10^{-3} m, a laser power of about 10^3 W is needed [3]. Above the threshold intensity for the appearance of the plasma, the penetration depth increases roughly linearly with increasing laser power [4].

To understand the welding process, it is important to know the dominating energy absorption mechanism and to answer questions like what keeps the keyhole open. Two processes of energy absorption are considered in the literature: the laser energy can be absorbed by the process of inverse bremsstrahlung in the keyhole plasma and then transported by plasma transport processes into the material [5–7], or the laser energy can be absorbed directly at the walls of the keyhole (Fresnel absorption) [8]. Without having a plasma in the keyhole but a neu-

tral gas, the keyhole is held open by the pressure arising from neutral atoms evaporating from the wall as is shown in [9]. This picture can change completely when a plasma is present, where a lot of pressure components contribute to the total pressure.

The keyhole plasma is a high pressure plasma, which fills a small volume and hence is influenced by the surrounding walls. Some attempts to investigate the keyhole plasma have already been made [5–7, 1,10–12]. However, the experimental results are obtained only for the plasma plume at the top of the keyhole [10–12] or for a half bounded plasma [1] and all theoretical models suffer from some shortcomings. The most sophisticated model given in [7] neglects radiative transport of excitations and excited states of neutral atoms and assumes a constant neutral gas temperature.

In the present paper we drop these restrictions. We give a radially symmetric model for the keyhole plasma with a fixed keyhole radius and consider the model for different incident laser powers. The only input parameters are the laser power and the keyhole radius. We solve the equations numerically and give all numerical results and material parameters for a cw CO_2 laser and iron.

The radial behavior of the hydrodynamic variables and some mean plasma quantities dependent on the incident laser power are obtained. The energy loss by radiative transport of excitations is calculated. The dominating energy transport mechanisms are determined and the results are discussed with respect to the application of laser welding.

In the following section we take a closer look at the expected transport mechanisms and describe our model. The hydrodynamic balance equations and their explicit form are given in the next section. Crucial for the self-

consistent model are the boundary conditions, contained in Sec. IV. Finally we discuss the results. The appendixes contain the explicit form of the source terms, some calculations connected with radiative transfer of excitations, and formulas for ionization and excitation rates.

II. THE SELF-CONSISTENT MODEL

The main ingredients of our plasma model were already stated in [7]. Here we give a short summary.

The transport mechanisms of the laser power into the material are illustrated in Fig. 1. The laser energy is absorbed by the process of inverse bremsstrahlung by the electrons. In the main part of the plasma, the plasma bulk, there is nearly no convective transport of ionization and thermal energy because of the high particle densities; just a small mean velocity of electrons and ions arises from a thermal diffusion effect. Therefore, the absorbed energy is transported by heat conduction and radiative transport of excitations towards the wall. Near the wall, in the so called presheath (for a review on the terms sheath, presheath, and Bohm criterion, see [13]) the electrons and ions are accelerated in the arising electric field. Only a small part of the laser energy is absorbed in the presheath. Consequently, by conservation of energy, the heat flux will decrease and the main transport mechanism becomes transport of ionization and thermal energy. In the small sheath with nonvanishing space charge density, the total energy flux, the particle fluxes, and the total pressure remain constant and hence a detailed description of the sheath is not necessary in our model. The electrons and ions recombine at the wall and their mass flux is compensated by evaporating neutral atoms.

We describe the presheath and the plasma bulk with stationary hydrodynamic balance equations. Quasineutrality and an isotropic pressure are assumed. Also, the plasma is considered to be ideal and to contain ions, electrons, ground state neutral atoms, and two excited states of neutral atoms. Doubly ionized iron atoms become important only for electron temperatures greater than about 1.6 eV. We will not get such high temperatures and consider therefore just singly ionized atoms.

It is assumed that the keyhole is radially symmetric and that the plasma quantities do not change in the direction of the keyhole axis (here the z axis). Of course, the laser energy is absorbed in the keyhole and, therefore, there is a trivial dependence on the z direction. Furthermore, the laser beam is affected by refraction, diffraction, and reflections at the wall while propagating through the keyhole. However, the real part of the refractive index will be shown to be nearly 1 at the center of the keyhole and the radius of the keyhole is about ten times greater than the laser wavelength. Therefore, the influence of refraction and diffraction on the laser beam should be small. The influence of reflections at the wall was investigated in [14] without considering a plasma. A considerable influence can arise for a long and narrow keyhole. Hence, the model should be best thought of to describe a small slice of the keyhole far enough from the surface for a keyhole with ratio of diameter to length of about 10.
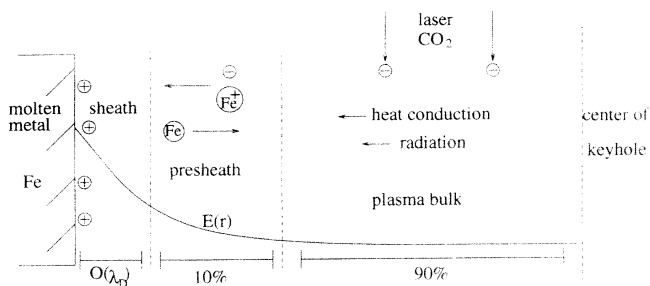

FIG. 1. The transport mechanisms in the keyhole plasma.

The main assumption made in the model to get the dominating collision terms is that the electron temperature is greater than approximately 5000 K or, equivalently, that the charged particle density is greater than about 10^{22} m^{-3}. This is consistent with all experimental data [1,10–12], when we assume that these results are also valid within the keyhole.

III. THE TRANSPORT EQUATIONS

A heuristic derivation of the transport coefficients and the hydrodynamic balance equations without excitations was given in [7]. Therefore, we simply state the equations and just mention some new features connected with excited states.

We use the notation $\nabla_r := d/dr$, where r is the distance from the center of the keyhole.

A. The continuity equations

The continuity equation for the ions and electrons reads in cylindrical coordinates

$$\frac{1}{r}\nabla_r(rnu) = C , \tag{1}$$

where n is the density of electrons and ions, u is the radial component of the electron-ion velocity, and C the source term, explicitly stated in Appendix A. C contains just electron impact ionization and ternary recombination because of the high electron density. No electric flux can arise in this planar model because of the radial symmetry. Consequently, because of quasineutrality ions and electrons possess the same mean velocity u. Also, the total particle flux has to vanish: $n_{n,1}u_{n,1} + nu = 0$, where $u_{n,1}$ is the mean velocity of the ground state neutral atoms and $n_{n,1}$ the ground state density.

We neglect the momentum of the excited states, which is a good approximation because of their low densities. This yields for the continuity equations of the excited atoms

$$0 = \frac{dn_{n,j}}{dt} = C_{ex,j}$$

with the source terms $C_{ex,j}$ (see Appendix A), the densities n_{nj} of the excited state j, and $j = 2,3$.

B. The momentum balances

We take as momentum balance for the charged particles

$$\nabla_r [nk(T_e+T)]+\frac{1}{r}\nabla_r(rnmu^2)=R \quad , \qquad (2)$$

where m is the mass of iron atoms and R the friction force (Appendix A). The left hand side of Eq. (2) contains the isotropic pressure $nk(T_e+T)$ of electrons and ions and their convective momentum flux. The temperatures of ions and neutral atoms, T, are assumed to be equal because of the strong interaction via charge exchange collisions, but they may differ from the electron temperature T_e. Because of momentum conservation no collision term appears in the total momentum balance:

$$\nabla_r[nk(T_e+T)]+\frac{1}{r}\nabla_r(rnmu^2)$$
$$=-\nabla_r(n_nkT)-\frac{1}{r}\nabla_r(rn_{n,1}mu_{n,1}^2) \quad , \qquad (3)$$

with $n_n=n_{n,1}+n_{n,2}+n_{n,3}$.

C. The energy balances

To determine the temperatures two energy balances are needed. The total energy balance is

$$\frac{1}{r}\nabla_r\left[r\left[q+q_e+nu\left[\frac{5}{2}kT_e+E_{\text{ion},1}+\frac{m}{2}u^2\right]\right.\right.$$
$$\left.\left.+n_{n,1}u_{n,1}\frac{m}{2}u_{n,1}^2\right]\right]=Q_{\text{tot}} \quad , \qquad (4)$$

where q is the sum of the radial ion and neutral heat flux, q_e is the radial electron heat flux, $E_{\text{ion},1}$ the ground state ionization energy, and Q_{tot} contains the absorbed laser energy via inverse bremsstrahlung and the energy transport by emitted and reabsorbed photons (Appendix A). The left hand side of Eq. (4) exhibits the possible hydrodynamic energy transport mechanism, namely, head conduction and convective transport of ionization, thermal, and kinetic energy. Later on we will see that the energy of the escaping photons is small compared with the other terms in Eq. (4). Hence, we do not have to worry about absorption or reflection at the wall and assume all escaping photons to be absorbed at the wall.

Considering neutral atoms and ions leads to

$$\frac{1}{r}\nabla_r\left[rq+rnu\frac{m}{2}(u^2-u_{n,1}^2)\right]-nueE=Q_{in} \quad , \qquad (5)$$

where Q_{in} contains the gain of energy by elastic collisions with electrons and the energy transport by photons (see Appendix A). The electric field E is obtained from the generalized Ohm's law $\nabla_r(nkT_e)=-neE$. We close the system of equations by giving expressions for the heat fluxes (see [7]). The electron heat flux q_e is determined from Fourier's law $q_e=-\lambda_e\nabla_rT_e$ with the electron thermal conductivity λ_e. Similarly, for the ion and neutral atom heat fluxes we choose

$$q:=q_i+q_n=-\lambda_i\nabla_rT-\lambda_n\nabla_rT=:-\lambda\nabla_rT \qquad (6)$$

with the thermal conductivities λ_i,λ_n of the ion and neutral atoms, respectively, and the sum of both λ.

D. Explicit form of the system

To get some insight into the structure of the equations we solve the system for the derivatives. We obtain with

$$C_{ei}:=C-nu/r, \quad C_n=-C-mn_{n,1}u_{n,1}/r \quad ,$$
$$R_{ei}:=R-mnu^2/r, \quad R_n:=-R-mn_{n,1}u_{n,1}^2/r$$

the explicit equations

$$\nabla_r u=\frac{u}{n[mu^2-k(T_e+T)]}\left[R_{ei}+nk\left[\frac{q_e}{\lambda_e}+\frac{q}{\lambda}\right]\right.$$
$$\left.-\frac{C_{ei}}{u}[mu^2+k(T_e+T)]\right] \quad , \qquad (7)$$

$$\nabla_r n=\frac{1}{u}(C_{ei}-n\nabla_r u) \quad , \qquad (8)$$

$$\nabla_r u_{n,1}=\frac{u_{n,1}}{n_{n,1}(mu_{n,1}^2-kT)}$$
$$\times\left[R_n+\frac{n_{n,1}kq}{\lambda}-\frac{C_n}{u_{n,1}}(mu_{n,1}^2+kT)\right] \quad , \qquad (9)$$

$$\nabla_r T_e=-q_e/\lambda_e, \quad \nabla_r T=-q/\lambda \quad , \qquad (10)$$

$$\nabla_r q_e=Q_{\text{tot}}-\frac{q_e}{r}-\frac{1}{r}\nabla_r\left[rq+rnu\right.$$
$$\left.\times\left[E_{\text{ion}}+\frac{5}{2}kT_e+\frac{m}{2}(u^2-u_{n,1}^2)\right]\right] \quad , \qquad (11)$$

$$\nabla_r q=Q_{in}-\frac{q}{r}-\frac{1}{r}\nabla_r\left[rnu\frac{m_i}{2}(u^2-u_{n,1}^2)\right]-u\nabla_r(nkT_e) \quad . \qquad (12)$$

Equation (7) indicates a singularity at the Bohm velocity $u_{\text{Bohm}}=\sqrt{k(T_e+T)/m_i}$ and Eq. (9) at the neutral atom thermal velocity $u_{n,\text{th}}=\sqrt{kT/m_i}$. Note that $\lambda_i,\lambda_n\ll\lambda_e$ because of the small electron mass. Therefore the heat flux of ions and neutral atoms q is expected to contribute not significantly to the total energy flux into the wall. However, the term $q_n/\lambda_n=-\nabla_r T$ in Eq. (9) and the term $q_e/\lambda_e=-\nabla_r T_e$ in Eq. (7) are of the same order of magnitude and both have therefore an influence on the velocities.

As already noted, the numerical solutions of the system (7)–(13) will show that the mean velocities can be neglected in the plasma bulk. In this case, the system (7)–(12) simplifies to the equations of heat conduction,

$$\nabla_r q_e+q_e/r+\nabla_r q+q/r=Q_{\text{tot}} \text{ and } \nabla_r q+q/r=Q_{in} \quad ,$$

and the total momentum balance $nk(T_e+T)+kTn_n$ =const, where the heat fluxes are given by the Fourier law. The densities are determined from Eq. (2) and $C=0$.

IV. BOUNDARY CONDITIONS

Seven boundary conditions (for n, T, T_e, q, q_e, u, and $u_{n,1}$) are necessary to determine the solution of Eqs. (7)–(12) uniquely. The conditions are given at $r = 0$, the center of the keyhole, and at r_{ps}, the presheath-sheath boundary. Some quantities remain constant in the small sheath (like the total pressure). For these quantities it is also possible to give boundary conditions at the wall ($r = r_w$).

The radial symmetry requires that the mean velocities and heat fluxes vanish at $r = 0$. Because the plasma is sustained from evaporating neutral atoms, vapor pressure of the neutral atoms is assumed at the presheath-sheath boundary; a formula for iron is given in [7]. Furthermore, the total pressure at the wall has to be atmospheric pressure p_0 plus the pressure γ/r_w due to the surface tension of the melt surrounding the keyhole to obtain mechanical stability [9]. Therefore we require that the sum of all pressure terms [see Eq. (3)] is equal to $p_0 + \gamma/r_w$, which is under normal conditions approximately 1.2×10^5 Pa. At the presheath-sheath boundary r_{ps}, the ions and electrons attain the Bohm velocity $u(r_{ps}) = u_{\text{Bohm}}$ [13], which indicates that a considerable charge density arises and the approximation of quasineutrality is not valid in the sheath. Finally, we specify the electron heat flux at the presheath-sheath boundary by choosing the electron distribution function f_e at $r = r_{ps}$ to be

$$f_e(v) = An(r_{ps}) \left[\frac{m_e}{2\pi k \tilde{T}_e} \right]^{1/2} \exp \left[-\frac{m_e v^2}{2k\tilde{T}_e} \right]$$

$$\text{for } v > -\sqrt{2e\phi/m_e}$$

and zero elsewhere, with the potential drop ϕ in the sheath [15]. A positive v means a velocity towards the wall. Therefore no electron emission from the wall and no reflections of electrons at the wall are assumed. The parameters A, ϕ, and $\tilde{T}_e$ may now be chosen in such a way that the first three moments of the distribution function f_e coincide with the quantities obtained from the transport equations. With $A = 2/[1 + \text{erf}(\sqrt{e\phi/k/\tilde{T}_e})]$ we get $\int f_e(v)dv = n(r_{ps})$. From $\int f_e(v)vdv \overset{!}{=} n(r_{ps})u_{\text{Bohm}}$ we obtain the potential drop ϕ in the sheath,

$$\int_{-\sqrt{2e\phi/m_e}}^{\infty} f_e(v)vdv = An(r_{ps})\sqrt{k\tilde{T}_e/2\pi m_e}$$

$$\times \exp \left[-\frac{e\phi}{k\tilde{T}_e} \right]$$

$$\overset{!}{=} n(r_{ps})\sqrt{k[T_e(r_{ps}) + T(r_{ps})]/m} .$$

The parameter $\tilde{T}_e$ is specified by the requirement that the temperature given by f_e is equal to the temperature obtained from the hydrodynamic balance equations:

$$m_e \int f_e(v)(v - u_{\text{Bohm}})^2 dv \overset{!}{=} n(r_{ps})kT_e(r_{ps}) .$$

Finally, we can calculate the electron heat flux q_e at the
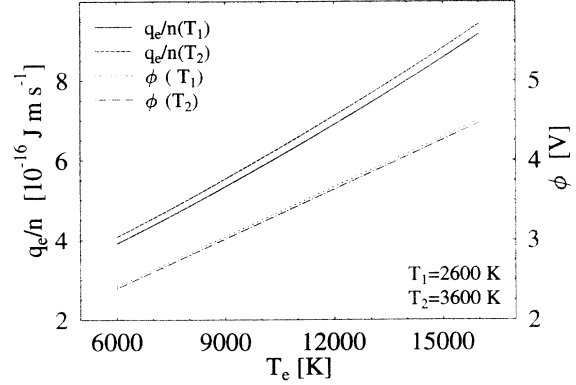

FIG. 2. The electron heat flux density at the wall divided by the electron density at the wall q_e/n and the potential drop in the sheath ϕ dependent on the electron temperature T_e for two different ion–neutral-atom temperatures T_1 and T_2.

presheath-sheath boundary from

$$q_e(r_{ps}) = \frac{m_e}{2} \int f_e(v)(v - u_{\text{Bohm}})^3 dv$$

$$= n(r_{ps}) \left[\frac{A}{2}\sqrt{2k\tilde{T}_e/\pi m_e}(k\tilde{T}_e + e\phi) \right.$$

$$\times \exp \left[-\frac{e\phi}{k\tilde{T}_e} \right]$$

$$\left. -\frac{3}{2}u_{\text{Bohm}}kT_e(r_{ps}) - \frac{m_e}{2}u_{\text{Bohn}}^3 \right] .$$

The quantity $q_e/n(r_{ps})$ depends on the electron and ion–neutral-atom temperature at the presheath-sheath boundary r_{ps} and is shown in Fig. 2.

V. RESULTS

In Fig. 3–Fig. 7 the radial behavior of some plasma quantities is shown. If not stated otherwise, the mean laser intensity $I_{\text{laser}} = \int_0^{r_w} I 2\pi r dr/(\pi r_w^2)$ is taken to be 2×10^{10} W m^{-2}. We take for the keyhole radius $r_w = r_{\text{laser}} = 10^{-4}$ m and normalize the radial coordinate to the keyhole radius. Note that just about 63% of the laser power enters the keyhole because of the assumed
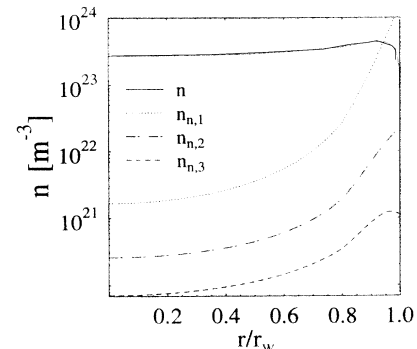

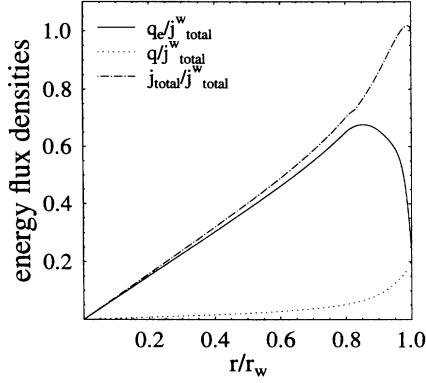FIG. 3. Radial dependence of the densities $n, n_{n,1}, n_{n,2}, n_{n,3}$.

MODEL OF A LASER HEATED PLASMA INTERACTING WITH . . .

FIG. 4. Radial dependence of the heat fluxes q_e and q and the total energy flux j_{total} normalized to the total energy flux at the wall j_{total}^w.

FIG. 6. Radial dependence of the velocities of electrons and ions and neutral particles. The plasma bulk with $u/u_{Bohm} \ll 1$ is not shown.

Gaussian profile of the laser intensity I (see Appendix A).

The ion-electron density (Fig. 3) is nearly constant in the plasma bulk because of the constant pressure and the high degree of ionization, while the neutral atom densities are increasing rapidly towards the wall. Since we neglected the mean velocities of the excited states, the densities of the excited states do not vanish at r_w. This would be expected by estimating the densities of the excited states in the neutral vapor at the wall from a Boltzmann distribution. However, the density of the second excited state $n_{n,3}$ decreases near the wall because of the decreasing electron temperature. The density of the ions and electrons decreases in the presheath by approximately a factor of 3 because of the rapidly increasing mean velocity (Fig. 6). In Fig. 4 the different energy density fluxes are shown normalized to the total energy density flux at the wall j_{total}, where

$$j_{total} = \left[q + q_e + nu \left(\frac{5}{2}kT_e + E_{ion,1} + \frac{m}{2}u^2 \right) + n_{n,1}u_{n,1}\frac{m}{2}u_{n,1}^2 \right]_{r=r_{ps}} .$$

As already noted, the energy transport in the plasma bulk is mainly governed by the electron heat flux. Near the wall the convective transport of ionization energy becomes important. Only in the presheath are the mean velocities significantly different from zero (Fig. 6). Near the wall, the ion–neutral-atom heat flux becomes more important because of the high neutral atom density. All temperatures decrease towards the wall (Fig. 5). At the center of the keyhole the electron and ion–neutral-atom temperatures depart by about 10% from each other. The difference increases towards the wall, where T_e is approximately twice T. Note that the vapor pressure was given as the boundary condition. This restricts the ion–neutral-atom temperature at the wall to a small range around 3000 K.

The energy emitted or absorbed by radiative transitions per time and volume is shown in Fig. 7. The first excited state gives just an emission of radiation in the whole plasma, increasing towards the wall, whereas the second excited state shows an emission of radiation in the plasma bulk and an absorption of radiation in the presheath. We remark that the radiative energy flux at r_w, which is approximately the area under the curves, is of the order of 1% of the total energy flux. The radiation arising from the excited states of the ions was not considered, even though they may give a significant contribution to the number of emitted photons because of the high ion density in the plasma bulk. However, the excit-
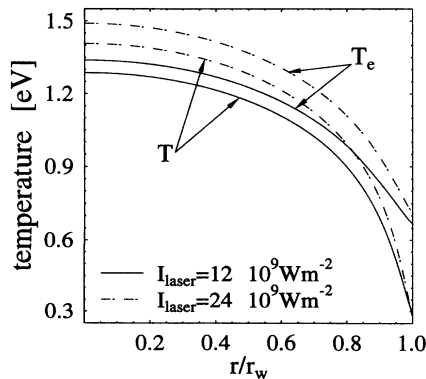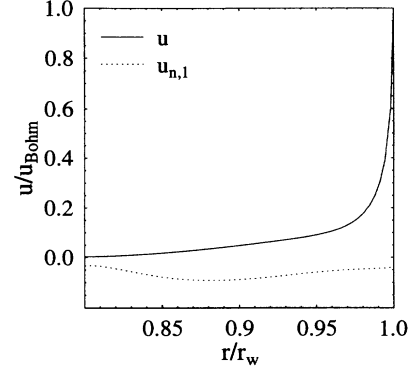

FIG. 5. Radial dependence of the electron and ion–neutral-atom temperatures T_e and T for two incident laser powers.
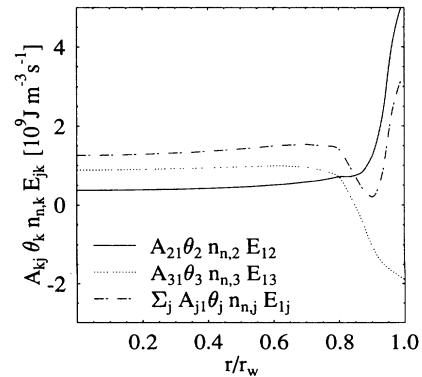

FIG. 7. Radial dependence of the source terms in Eq. (4) connected with radiative transfer for the first and second excited states and the sum of both.
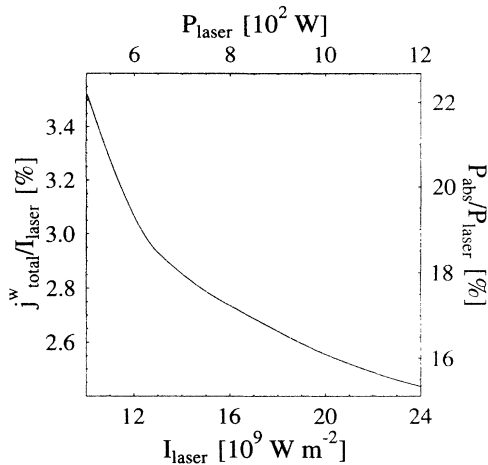
FIG. 8. The total energy flux at the wall j^w_{total} divided by the mean laser intensity I_{laser} over the mean laser intensity. Alternatively, the absorbed laser power P_{abs} divided by the incident laser power P_{laser} depending on the incident laser power for a 1 mm deep keyhole is shown.

ed ion states have only small transition probabilities. Hence, the influence of radiative transport of excitations on the energy transport towards the wall is small.

The dependence of some mean plasma quantities on the incident laser intensity is shown in Fig. 8–Fig. 10. The mean electron temperature (Fig. 10) is increasing because of an increasing heat flux q_e (see also Fig. 5). The ion–neutral-atom temperature then follows the electron temperature. The pressure is given as the boundary condition and is nearly constant in the whole keyhole. Therefore the electron density at the center decreases (Fig. 9) and the degree of ionization increases, or equivalently the neutral-atom density decreases. A decreasing electron density and increasing electron temperature lead to a decreasing degree of absorbed energy (Fig. 8). Extrapolating the results to a 10^{-3} m deep keyhole, about 20% of the incident laser power will be absorbed. Considering only the laser power which enters the keyhole, the degree of absorption is about 30%.

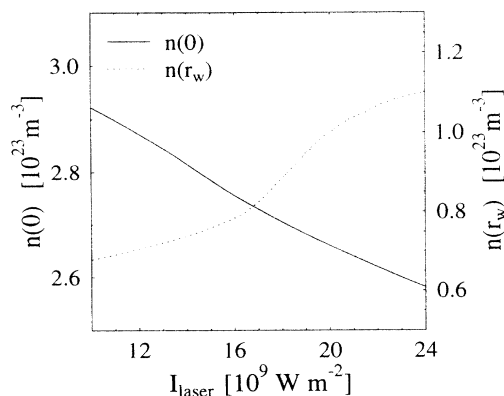For a half bounded plasma, experiments give values of

FIG. 9. The charged particle density at the wall $n(r_w)$ and at the center of the keyhole $n(0)$ depending on the mean laser intensity.
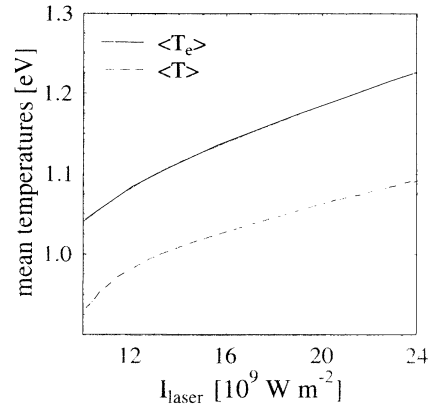

FIG. 10. The mean electron and ion–neutral-atom temperature $\langle T_e \rangle$ and $\langle T \rangle$ depending on the mean laser intensity.

0.8–1 eV and 10^{23}–3×10^{24} m^{-3} [1]. For the plasma plume at the top of the keyhole near the surface, electron densities of about 10^{23} m^{-3} and electron temperatures of 0.6 eV were measured [12,11]. The difference of our results from the last cited results may be expected because of the plasma cooling by the surrounding atmosphere, which is absent within the keyhole.

To apply our results to the process of laser keyhole welding, it should be noted that the assumed keyhole form may restrict the model to low welding speed. In addition, the model cannot give correct quantities near the top of the keyhole (see above), because we have neither considered the ambient gas nor have we taken into account heat fluxes or mean velocities in the direction of the keyhole axis.

VI. SUMMARY AND CONCLUSIONS

Hydrodynamic balance equations for the keyhole plasma were set up and solved. Electrons, ions, and three excited states were considered. Quasineutrality and equal ion and neutral atom temperature were assumed and the momentum of the excited neutral atoms was neglected. As boundary conditions the total pressure and the vapor pressure were given at the wall and the electron heat flux and the Bohm velocity at the presheath-sheath boundary. The solutions of the transport equations suggested dividing the quasineutral region of the plasma into the plasma bulk and the presheath, where heat conduction and convective transport of ionization energy were the dominating transport mechanisms, respectively. While the electron temperature was about twice the ion–neutral-atom temperature near the wall, at the center of the keyhole the temperatures differ by less than 10% from each other because of the high charged particle density. Since the transport of excitation energy by photons was small compared to the total energy flux, the main reason for the plasma bulk not being in a local thermodynamic equilibrium was the strong electron heat flux. The small influence of the radiation arises from the fact that the keyhole plasma occupies a small volume and the number of emitted photons is approximately proportional to this volume. However, the emitted radiation can be used for

experimental diagnostics when the radially emitted radiation is measured as in [1].

Calculations with different incident laser powers and a fixed keyhole radius were carried out. For an incident laser power of about 10^{10} W m^{-2} the mean electron temperature and the mean charged particle density were obtained to be about 1.1 eV and 3×10^{23} m^{-3}, which fits in the range of values measured in [1].

Compared with the simpler model in [7] we got a lower electron temperature and a higher ion–neutral-atom temperature because of the higher ionization rate and the variable ion–neutral-atom temperature, respectively. Nevertheless, the main transport mechanisms are obtained to be the same.

Applied to laser keyhole welding, we conclude that the keyhole plasma contributes significantly to the energy transport from the laser into the material.

ACKNOWLEDGMENTS

APPENDIX A: THE SOURCE AND COLLISION TERMS AND TRANSPORT COEFFICIENTS

The continuity equation Eq. (1) contains the source term

$$C = \sum_{j=1,2,3,} (\alpha_{\text{ion},j} n_{n,j} n - \alpha_{\text{coll},j} n^3) \, ,$$

where $\alpha_{\text{ion},j}$ and $\alpha_{\text{coll},j}$ are the electron impact ionization and ternary recombination rates from and into state j, respectively. The source terms for the excited states have to contain also excitation, quenching, and radiative transitions:

$$C_{\text{ex},j} = - A_{j1} \theta_j n_{n,j} - n_{n,j} n \alpha_{j,1} + n_{n,1} n \alpha_{1,j}$$
$$- \alpha_{\text{ion},j} n_{n,j} n + \alpha_{\text{coll},j} n^3 \, ,$$

with the electron impact excitation or quenching rate $\alpha_{k,j}$ from k into state j, the rate of spontaneous transition A_{jk} from state j into state k, and θ_j explained in Appendix B. In the case of a homogeneous plasma, θ_j gives approximately the effective lifetime of a photon [16]. Some formulas for the ionization and excitation rates are given in Appendix C and some remarks on radiative transport of excitation and special features of the iron spectrum can be found in Appendix B. The dominant terms in the friction force R are the charge exchange collisions,

$$R = \sum_{j=1,2,3} (\alpha_{\text{ion},j} n_{n,j} n m u_{n,j} - \alpha_{\text{coll},j} n^3 m u)$$
$$- \kappa_{in} m n_{n,1} n (u - u_{n,1}) - \kappa_{en} m_e n_{n,1} n (u - u_{n,1}) \, ,$$

where m_e is the electron mass, κ_{in} the rate for charge exchange collisions, and κ_{en} the rate for elastic neutral-atom–electron collisions. The right hand side of the total energy balance Q_{tot} contains just the absorbed laser energy and the escaping photons,

$$Q_{\text{tot}} = a_\omega I - \sum_{j=2,3} A_{j1} \theta_j n_{n,j} \hbar \omega_{j1} \, ,$$

where a_ω is the inverse bremsstrahlung absorption coefficient, and $\hbar \omega_{j1}$ the photon energy emitted from state j. The laser intensity I is assumed to have a Gaussian profile $I = [P_{\text{laser}} / (\pi r_{\text{laser}}^2)] \exp(-r^2 / r_{\text{laser}}^2)$ with the laser beam radius r_{laser} and the laser power in the considered slice of the keyhole P_{laser}. The elastic ion-electron and neutral-atom–electron collisions are exhibited in the ion–neutral-atom energy balance,

$$Q_{in} = \frac{m_e}{m} \frac{3nk(T_e - T)}{\tau_e}$$
$$+ \frac{m_e}{m} \kappa_{en} n_{n,1} n \left[\frac{3}{2} k(T_e - T) + \frac{m}{2} (u - u_{n,1})^2 \right]$$
$$- \sum_{j=2,3} A_{j1} \theta_j n_{n,j} \hbar \omega_{j1}$$

with the mean electron-electron collision time τ_e [17, p. 191].

It remains to specify the thermal conductivities. We choose for the electrons

$$\lambda_e^{-1} = \lambda_{e,e}^{-1} + \lambda_{e,n}^{-1} \, ,$$

where

$$\lambda_{e,e} = \frac{5}{2} \tau_e 1.28 \frac{n_e k^2 T_e}{m_e} \quad \text{and} \quad \lambda_{e,n} = \frac{1}{n_n \kappa_{en}} \frac{5}{2} \frac{n_e k^2 T_e}{m_e} \, .$$

The thermal conductivity $\lambda_{e,e}$ arises from electron-ion electron-electron collisions, whereas $\lambda_{e,n}$ arises from elastic electron–neutral-atom collisions. Similarly, for ions and neutral atoms we take

$$\lambda_i^{-1} = \lambda_{i,i}^{-1} + \lambda_{i,n}^{-1} \quad \text{and} \quad \lambda_n^{-1} = \lambda_{n,n}^{-1} + \lambda_{n,i}^{-1} + \lambda_{n,e}^{-1} \, ,$$

where the thermal conductivities $\lambda_{\alpha,\beta}$ arise from collisions of particle α with particle β and are given by

$$\lambda_{\alpha,\beta} = \frac{1}{n_\beta \kappa_{\alpha\beta}} \frac{5}{2} \frac{n_\alpha k^2 T_\alpha}{m_\alpha} \, .$$

The most important heat flux in our model is q_e and the dominating elastic collisions are Coulomb collisions. Hence, we used for the heat conductivity $\lambda_{e,e}$ a precise expression obtained from the Grad expansion [17, p. 247].

APPENDIX B: RADIATIVE TRANSPORT OF EXCITATIONS AND SOME SPECIAL FEATURES OF THE IRON SPECTRUM

An excited atom can undergo a spontaneous transition in its ground state by emitting a photon. This photon can be readsorbed from another atom or can escape to outside the plasma. Therefore, connected with radiative transport of excitations is an energy transport and an influence on the densities of excited states.

For a plasma with neutral atom ground state density $n_{n,1}$ and one excited state $n_{n,2}$ the balance equation or Biberman-Holstein equation for $n_{n,2}$ is

$$\frac{dn_{n,2}}{dt}(\mathbf{r}) = -n_{n,2}(\mathbf{r})A_{21} + \int_V n_{n,2}(\mathbf{r}')A_{21}H(\mathbf{r},\mathbf{r}')d^3r' \ ,$$

(B1)

where A_{21} is the rate of spontaneous transitions from state 2 into state 1 and $H(\mathbf{r},\mathbf{r}')d^3r'$ is the probability, that a photon emitted at $\mathbf{r}$ is absorbed at $\mathbf{r}'$ [16,18]. The integral term gives the rate of absorbed photons at the point $\mathbf{r}$ emitted in the volume V and the term $dn_{n,2}/dt$ may be thought to contain all other collision terms. We will see that radiative transfer has only a small influence on the plasma quantities. Therefore, we perform a zeroth order perturbation calculation, i.e., we calculate the right hand side of (B1) with given densities and do not have to solve the complicated integral equation (B1). The right hand side of Eq. (B1) was abbreviated in previous sections to $A_{21}\theta_2 n_{n,2}$ with the integral operator θ_2 acting on $n_{n,2}$. The integral kernel H is given by

$$H(\mathbf{r},\mathbf{r}') = \frac{1}{4\pi|\mathbf{r}-\mathbf{r}'|^2}\int_{-\infty}^{\infty} \varepsilon_\omega(\mathbf{r}')k_\omega(\mathbf{r})e^{-\tau}d\omega \ , \quad \text{(B2)}$$

with $\tau = \int_{\mathbf{r}}^{\mathbf{r}'}k_\omega(\mathbf{r}'')d\mathbf{r}''$, where $\mathbf{r}''$ runs over the line $\mathbf{r}$-$\mathbf{r}'$.

The spectral line shape ε_ω and the absorption coefficient k_ω are given by

$$\varepsilon_\omega = \frac{\gamma_{12}}{2\pi[(\omega-\omega_{12})^2+(\gamma_{12}/2)^2]} \ ,$$

$$k_\omega = \frac{k_0}{1+(\omega-\omega_{12})^2(2/\gamma_{12})^2} \ ,$$

with the spectral linewidth γ_{12}. The absorption coefficient at the center of the line k_0 is

$$k_0 = \frac{1}{4}\lambda_{12}^2\frac{g_2}{g_1}A_{21}\frac{2}{\pi\gamma_{12}}n_{n,1} \ ,$$

where λ_{12} is the corresponding wavelength and g_k is the statistical weight of the state k.

The line shape and the absorption coefficient are given for purely collisional line broadening, which is a good approximation because of the high particle densities. For charged particle densities greater than 10^{22} m^{-3} the Stark effect is the main broadening mechanism [19]. There are only a few papers existing which have dealt with the measurement or calculation of the radiation linewidth γ for iron arising from the Stark effect [19,20]. Unfortunately, no experimental data were given for the lines considered here. Therefore, we used an estimate given in [21] which yields

$$\gamma_{12} \approx 3.3n\left[\frac{kT_e}{m_e}\right]^{1/6}\left[\frac{e^2a_0^3}{\epsilon_0\hbar}f_{12}\right]^{2/3}\left[\frac{\mathcal{R}}{E_{12}}\right]^{4/3} \ ,$$

where a_0 is the Bohr radius, ϵ_0 the permittivity of vacuum, and $\mathcal{R}$ the Rydberg constant. The keyhole plasma is highly inhomogeneous; in particular, the densities of the neutral atoms and excited atoms change by some orders
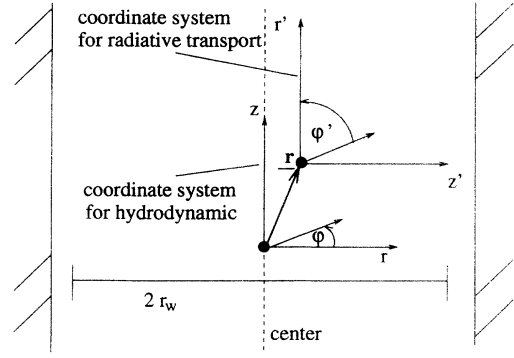

FIG. 11. The coordinate system for the evaluation of radiative transport.

of magnitude. However, the charged particle density varies only slightly and therefore is assumed to be constant, which yields $\gamma = $const. Now, k_ω can be written as $k_\omega(\mathbf{r})=\chi_0 n_{n,1}(\mathbf{r})$, where χ_0 does not depend on $\mathbf{r}$ and the integral in (B2) can be evaluated as

$$H(\mathbf{r},\mathbf{r}') = \frac{\chi_0 n_{n,1}(\mathbf{r})}{4\pi|\mathbf{r}-\mathbf{r}'|^2}e^{-\tau/2}[I_0(\tau/2)-I_1(\tau/2)] \ ,$$

where I_j are the modified Bessel functions of j's order.

To simplify the integral in (B1), we assume a planar keyhole geometry and introduce cylindrical coordinates as illustrated in Fig. 11. The origin of the coordinate system is put at the point $\mathbf{r}$. All quantities should vary only in the z' direction. This yields for τ

$$\int_{\mathbf{r}}^{\mathbf{r}'}k_\omega(\mathbf{r}'')d\mathbf{r}'' = \chi_0\frac{\sqrt{r'^2+z'^2}}{z'}\int_0^{z'}n_{n,1}(t)dt \ .$$

Going back to the coordinates used in the hydrodynamic calculations, where r is the distance from the center of the keyhole, we obtain

$$\int_V n_{n,2}(\mathbf{r}')H(\mathbf{r},\mathbf{r}')d^3r' = \int_{-r_\omega}^{r_\omega} d\psi\, n_{n,2}(|\psi|)$$

$$\times J\left[\frac{\chi_0}{2}\left|\int_r^\psi n_{n,1}(|t|)dt\right|\right]$$

$$\times \frac{\chi_0 n_{n,1}(r)}{4} \quad \text{(B3)}$$

with

$$J(z) = \int_z^\infty \frac{\exp(-t)}{t}[I_0(t)-I_1(t)]dt \ .$$

The last integral can be evaluated by series expansion,

$$J(z) \approx \begin{cases} -\ln(z)+\displaystyle\sum_{j=0} a_j z^j & \text{for } z < 3.75, \\[2ex] \dfrac{1}{z^{3/2}}\left[\displaystyle\sum_{j=0} b_j z^{-j}\right] & \text{for } z > 3.75, \end{cases}$$

with some numerical constants a_j and b_j. The remaining two integrations in (B3) cannot be done analytically because the densities depend on the integration variables.

The iron spectrum is one of the best known and contains some thousand lines. It was not at all the objective

TABLE I. The oscillator strengths f_{ik}, excitation energy E_{1j} (eV), ionization energy $E_{\mathrm{ion},j}$ (eV), and the statistical weights g_j of the three neutral atom states and the ion ground state.

State	f_{1j}	E_{1j} (eV)	$E_{\mathrm{ion},j}$ (eV)	g_j
1			7.1	81
2	0.17	3.3	3.3	170
3	0.33	4.9	3.0	75
Ion				58

of this work to consider all of them. Therefore, we coarse grained the iron spectrum (see [22]). From an atomic energy level diagram (see, e.g., [23]) it can be obtained that the spectrum can be approximated by a three level system with no transitions between the two excited states. In Table I we give the statistical weights of the levels and the averaged excitation energy and oscillator strength. The oscillator strength f_{jk} is related to the Einstein coefficient A_{kj} is

$$A_{kj} = f_{ij} \frac{2e^2 \omega_{kj}^2 g_j}{4\pi\epsilon_0 m_e c^3 g_k} , \qquad (B4)$$

where c is the speed of light.

APPENDIX C: IONIZATION AND EXCITATION RATES

The rates for elastic collisions were obtained by averaging the transport cross section of the considered collision over a Maxwellian distribution and are already given in [7]. Therefore we need to give only excitation and ionization rates. The recombination and quenching rates can then be obtained by a detailed balance relation.

The ionization cross sections given in [24] lead to the ionization rate from state j,

$$\alpha_{\mathrm{ion},j} = 8\pi a_0^2 \sqrt{2kT_e/\pi m_e}\, \xi_j \left[\frac{E_{\mathrm{ion},H}}{E_{\mathrm{ion},j}} \right]^2$$

$$\times \psi_1 \left[\frac{E_{\mathrm{ion},j}}{kT_e} \right] ,$$

with $E_{\mathrm{ion},H}$ the ionization energy of the hydrogen atom and the number of equivalent electrons ξ_j. The function ψ_1 is given by

$$\psi_1(t) = \int_t^\infty e^{-x} G\left[\frac{x}{t} \right] x\, dx$$

and

$$G(u) = \frac{1}{u} \left[\frac{u-1}{u+1} \right]^{3/2}$$

$$\times \left[1 + \frac{2}{3} \left[1 - \frac{1}{2u} \right] \ln(2.7 + \sqrt{u-1}) \right] .$$

The recombination rate can be obtained from a detailed balance relation [22]

$$\alpha_{\mathrm{coll},j} = \frac{g_k}{2g_{\mathrm{ion}}} \left[\frac{h^2}{2\pi m_e kT_e} \right]^{3/2} \exp\left[\frac{E_{\mathrm{ion},j}}{kT_e} \right] \alpha_{\mathrm{ion},j} .$$

For the excitation cross section we used the formula from Drawin [25] and obtained for the excitation rate

$$\alpha_{j,k} = 8\pi a_0^2 \left[\frac{\mathrm{Ry}}{E_{kj}} \right]^2 f_{jk} \sqrt{2kT_e/\pi m_e}\, \frac{E_{kj}}{kT_e}$$

$$\times \psi_2 \left[\frac{E_{kj}}{kT_e} \right] ,$$

with the excitation energy E_{kj} and

$$\psi_2(t) = \int_t^\infty \left[1 - \frac{t}{x} \right] e^{-x} \ln\left[1.25 \frac{x}{t} \right] dx .$$

The rate of quenching is given by [22],

$$\alpha_{k,j} = \frac{g_j}{g_k} \exp\left[\frac{E_{kj}}{kT_e} \right] \alpha_{j,k} .$$

[1] W. Sokolowski, G. Herziger, and E. Beyer, in *High Power Lasers and Laser Machining Technology*, edited by A. Quenzer, SPIE Proc. Vol. 1132 (SPIE, Bellingham, WA, 1989), pp. 288–295.

[2] J. Mazumder, in *Laser Materials Processing*, edited by M. Bass (North-Holland, Amsterdam, 1983).

[3] E. Beyer, L. Bakowsky, R. Poprawe, and G. Herziger, in *Industrial Applications of High-Power Lasers, Linz, Austraia, 1983*, edited by J. S. Ready, SPIE Proc. Vol. 455 (SPIE, Bellingham, WA, 1984), pp. 75–80.

[4] J. G. Allman, *Laser-Beam Interactions with Materials* (Springer, Berlin, 1989).

[5] J. Dowden, P. Kapadia, and N. Postacioglu, J. Phys. D 22, 741 (1989).

[6] B. R. Finke, P. D. Kapadia, and J. M. Dowden, J. Phys. D 23, 643 (1990).

[7] C. Tix and G. Simon, J. Phys. D 26, 2066 (1993).

[8] W. Schulz, G. Simon, and M. Vicanek, J. Phys. D 19, L173 (1986).

[9] J. Kroos, U. Gratzke, and G. Simon, J. Phys. D 26, 474 (1993).

[10] A. Poueyo, L. Sabatier, G. Deshors, R. Fabbro, A. M. de Frutos, D. Bermejo, and J. M. Orza, J. Phys. IV (France) Colloq. 1, C7-183 (1991).

[11] Z. Szymański, J. Kurzyna, and W. Kalita, in *Proceedings of the XXI International Conference on Phenomena in Ionized Gases*, edited by J. Böseler, G. Ecker, and U. Arendt (AG Plasmaphysik, Bochum, 1993), Vol. II, pp. 265–266.

[12] A. Poueyo-Verwaerde, R. Fabbro, G. Deshors, A. M. de Frutos, and J. M. Orza, J. Appl. Phys. 74, 5773 (1993).

[13] K.-U. Riemann, J. Phys. D 24, 493 (1991).

[14] A. G. Borkin *et al.*, Kvant. Elektron. (Moscow) 12, 2300 (1985) [Sov. J. Quantum Electron. 15, 1515 (1985)].

[15] G. A. Emmert, R. M. Wieland, A. T. Mense, and J. N.

Davidson, Phys. Fluids **23**, 803 (1980).

[16] L. M. Biberman, Zh. Eksp. Teor. Fiz. **17**, 416 (1947) [Sov. Phys. JETP **17**, 416 (1947)].

[17] R. Balescu, *Transport Processes in Plasmas* (North-Holland, Amst⁻ ₋am, 198₆, ₋₋₋ ₋.

[18] T. Holstein, Phys. Rev. **72**, 1212 (1947).

[19] A. Lesage, J. L. Lebrun, and J. Richou, Astrophys. J. **360**, 737 (1990).

[20] J. Purić, A. Srećković, S. Djeniže, S. Bukvić, S. Pivalica, and J. Labat, in *Proceedings of the XXI International Conference on Phenomena in Ionized Gases* [11], Vol. I, pp.

263–264.

[21] I. I. Sobelman, L. A. Vainshtein, and E. A. Yukov, *Excitation of Atoms and Broadening of Spectral Lines* (Springer, Berlin, 1981).

[22] L. M. Biberman, V. S. Vorob'ev, and I. T. Yakubov, *Kinetics of Nonequilibrium Low-Temperature Plasmas* (Consultants Bureau, New York, 1987).

[23] A. A. Radzig and B. M. Smirnov, *Reference Data on Atoms, Molecules, and Ions* (Springer, Berlin, 1982).

[24] M. Gryzinski, Phys. Rev. **138**, A305 (1965).

[25] H. W. Drawin, Z. Phys. **225**, 483 (1969).